Field-induced evolution of magnetic ordering in the quantum spin system (CuBr)$Sr_2Nb_3O_{10}$ with a 1/3 magnetization plateau

C. Ritter
Institut Laue-Langevin, Boite Postale 156, 38042 Grenoble Cedex, France

S. M. Yusuf* and A. K. Bera†
Solid State Physics Division, Bhabha Atomic Research Centre, Mumbai 400 085, India

Y. Goto, C. Tassel, and H. Kageyama
Department of Energy and Hydrocarbon Chemistry, Graduate School of Engineering, Kyoto University, Nishikyo, Kyoto 615-8510, Japan

A. M. Arévalo-López and J. P. Attfield
Centre for Science at Extreme Conditions and School of Chemistry, University of Edinburgh, Edinburgh EH9 3JZ, UK
(Received 15 May 2013; published 3 September 2013)

The field-induced evolution of the magnetic ordering in (CuBr)$Sr_2Nb_3O_{10}$ with a 1/3 magnetization plateau has been investigated by neutron diffraction under magnetic fields up to 10 T. With an increasing magnetic field, the zero-field helical antiferromagnetic (AFM) phase, AF1, with $\kappa = [0\ 3/8\ 1/2]$ is replaced by a simple ferromagnetic phase with $\kappa = [0\ 0\ 0]$, the formation of which is, however, retarded by the appearance of a second AFM, AF2, with $\kappa = [0\ 1/3 \sim 0.46]$. Upon further increasing of the magnetic field, the AF2 phase disappears and only the ferromagnetic phase persists. The results clearly show that the magnetization plateau, induced by the competition between field-induced ferromagnetic, F, and AF2 phases, is coincidentally situated at $M = 1/3\ M_S$ of the dc magnetization curve. The AF1 and AF2 phases have strongly differing magnetic propagation vectors and are therefore not directly related.

DOI: 10.1103/PhysRevB.88.104401 PACS number(s): 75.30.Kz

I. INTRODUCTION

Several members of the Dion-Jacobson series of compounds (CuX)$A_{n-1}B_nO_{3n+1}$ (X = Halide, A = La, Ca, Sr, Ba, and B = Nb, Ta, Ti) have lately been studied intensively as far as their crystal structure and magnetic behavior are concerned.[1–6] Originally described in $P4/mmm$,[7,8] the crystal structure of these compounds is characterized by square lattices of Cu^{2+} ions in CuX-Halide layers separated by n slabs of nonmagnetic corner-sharing BO_6 octahedra. Interest in these compounds was stimulated as the compounds were believed to represent possible examples for the frustrated two-dimensional (2D) $S = 1/2$ square lattice J_1-J_2 model.[9,10] Recently it was shown, however, that the crystal structures of the $n = 2$ compounds (CuCl)$LaNb_2O_7$ (Refs. 1 and 11), (CuBr)$LaNb_2O_7$ (see Ref. 4), and (CuCl)$LaTa_2O_7$ (see Ref. 5) do not possess a tetragonal symmetry but have a small orthorhombic distortion introducing a manifold of different magnetic interactions going far beyond the simple J_1-J_2 model. The strongest magnetic coupling (J_4) was shown to connect the fourth-nearest Cu^{2+} neighbors in these compounds. The compound (CuCl)$LaNb_2O_7$ shows a nonmagnetic spin gap ground state and was described as a ferromagnetic Shastry Sutherland compound with spin dimers being about 8.5 Å apart.[1,9,12] The appearance of magnetically long-range ordered states in (CuBr)$LaNb_2O_7$ and (CuCl)$LaTa_2O_7$ was linked to the increasing ratio between the sum of the numerous magnetic interdimer couplings and the intradimer coupling J_4 (see Ref. 5). The coupling between the 2D quasisquare lattice CuX layers through the nonmagnetic slabs of BO_6 octahedra is strong enough to lead to a three-dimensional long-range magnetic order in these $n = 2$ compounds.

Going to members of the Dion-Jacobson series that have $n = 3$, the coupling between the CuX layers should be further reduced as the 2D character of the magnetic CuX layers is increased by adding an additional nonmagnetic perovskite unit between the layers. Specific heat and magnetization measurements on (CuBr)$Sr_2Nb_3O_{10}$ revealed, however, a unique magnetic behavior with the existence of two magnetic phase transitions at zero field and—most surprising—the existence of a magnetization plateau at 1/3 of the saturation magnetization (M_S).[13] While magnetization plateaus at $M = 1/3\ M_S$ are predicted for lattices based on triangular symmetries,[14] the frustrated square lattice with $S = 1/2$ should only allow a plateau at $M = 1/2\ M_S$ within the simple J_1-J_2 model.[15] Our first study on this compound using neutron diffraction determined the zero-field magnetic structure below $T_{N1} = 7.5$ K to consist of an antiferromagnetic (AFM) alignment of Cu spins within the CuBr layers (helical magnetic structure) with a magnetic propagation vector $\kappa = [0\ 3/8\ 1/2]$ and a magnetic moment value of about $\mu_{Cu} = 0.8(1)\ \mu_B$ at 2 K.[6] In order to explain the existence of the helical magnetic structure not foreseen in the J_1-J_2 model, the J_1-J_2-J_3 was invoked. Interestingly enough, a 1/3 plateau in the magnetization has been theoretically predicted within the J_1-J_2-J_3 model for $J_1 = -1$, $J_2 = 1$, and $J_3 = 0.5$ (see Ref. 16). No long-range magnetic order was found in the temperature range between $T_{N1} = 7.5$ K and 9 K, where the specific heat data[13] showed a first magnetic phase. Earlier preliminary neutron-diffraction data under a magnetic field of 4.5 T (corresponding to the 1/3 magnetization plateau state) indicated the presence of a different magnetic propagation vector under the field without explaining the existence of the 1/3 magnetization plateau.[6]

In this paper, we present the results of a recent neutron-diffraction investigation under magnetic fields up to 10 T. The results clearly show that the magnetization plateau is induced by the competition between two field-induced magnetic phases (a ferromagnetic, F, phase and a AFM, AF2, phase with $\kappa = [0\ 1/3\ \gamma]$) and is only coincidentally situated at $M = 1/3\ M_S$.

II. EXPERIMENTAL PROCEDURES

The sample of $(CuBr)Sr_2Nb_3O_{10}$ was prepared, as described previously,[8] by a low-temperature ion-exchange reaction between the parent compounds $RbSr_2Nb_3O_{10}$ and $CuBr_2$. Neutron-diffraction data were taken at room temperature (RT) and at 20 K on the high-resolution powder diffractometer D2B ($\lambda = 1.594$ Å, $\boldsymbol{Q} = 0.2$–7.7 Å^{-1}) at the Institut Laue Langevin (ILL), Grenoble, France, in order to check for the symmetry and the purity of the compound. High-intensity powder-diffraction data were recorded on the high flux instrument D20 as well, installed at the ILL ($\lambda = 2.419$ Å, $\boldsymbol{Q} = 0.25$–4.8 Å^{-1}) as a function of temperature and magnetic field. Long measurements of 6 hours each were taken at 2 K for magnetic field values of $H = 0$, 1, 2.5, 4.5, 5.5, and 10 T. Additional scans were taken at zero field at 8.5, 15, and at 26 K and for $H = 4.5$ T at 5.5 and 8.5 K in order to verify the magnetic phase diagram proposed by Tsujimoto *et al.*[13] Low temperatures and magnetic fields up to 10 T were achieved using an Oxford Instruments horizontal cryomagnet. A radially oscillating collimator was used to suppress the scattering of the cryomagnet. The sample was put inside a cylindrical vanadium sample holder in the form of pressed pellets in order to avoid any reorientation of powder grains under the effect of the magnetic field. The diffraction data were analyzed by the Rietveld method using the FULLPROF suite of programs.[17] Magnetic symmetry analysis was done using the Program BASIREPS, which is included in the FULLPROF suite.[18,19]

III. RESULTS AND DISCUSSION

A. Crystal structure

The crystal structure of $(CuBr)Sr_2Nb_3O_{10}$ has been reinvestigated by high-resolution neutron diffraction using the D2B diffractometer. Such a high-resolution diffraction pattern measured at RT is shown in Fig. 1. The data were first refined in space group $P4/mmm$ using the previously published crystal structure model.[8] There is no evidence of a peak splitting as the unit cell parameters stay metrically tetragonal at RT and at 20 K. The refinement, however, leads to extremely elevated isotropic displacement parameters U_{iso} for the bromine atom at the Wykoff position $1d$ and for the oxygen atom (O1) at the Wykoff position $2f$. The high value of U_{iso} for the bromine position had been already found by Tsujimoto *et al.*[8] from x-ray diffraction (XRD), whereas the same phenomena had not been determined for O1 as a single isotropic displacement parameter had been used for all four oxygen atoms, hiding thereby the unusual behavior of O1. The left inset of Fig. 1 displays part of the refined diffraction pattern at relatively high two-theta values (range ~100–140°) where inconsistencies between the published model[8] and the data become clearly visible. A high atomic displacement factor (ADP) of the

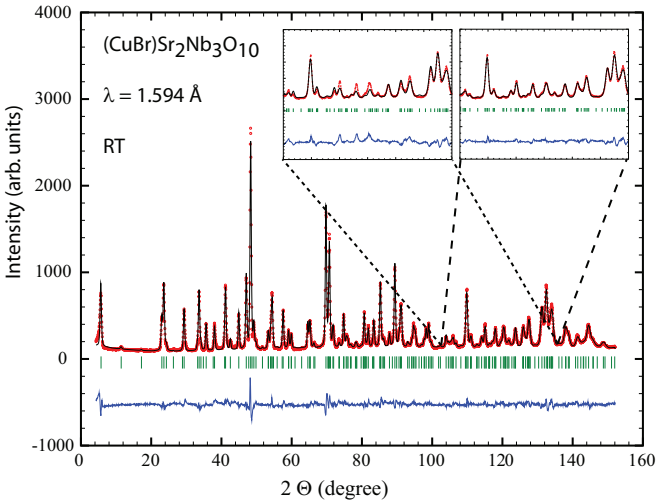

FIG. 1. (Color online) Observed (red points), calculated (black line), and difference patterns (blue line at the bottom) of $(CuBr)Sr_2Nb_3O_{10}$ at room temperature refined in $P4/mmm$ with Br and O1 on split positions $4o$ and $4n$, respectively. The tick marks indicate the calculated positions of the Bragg peaks. The right inset shows an enlarged view of the region between $2\Theta \sim 100$–$140°$ of the refinement. The left inset shows the same region for a refinement using the model of Ref. 8 with Br on $1d$ and O1 on $2f$.

halide was found in the $n = 2$ compound $CuBrLaNb_2O_7$ and had been interpreted[4] as indicating the splitting of the Br position, with the major shift appearing within the Cu-Br layer. Consistently, when allowing a splitting of the Br position [$1d$; ($1/2$, $1/2$, $1/2$)] into either the $4o$ (x, $1/2$, $1/2$) or the $4k$ (x, x, $1/2$) positions, a clear improvement in the refinement of the present $(CuBr)Sr_2Nb_3O_{10}$ pattern is achieved. Both $4o$ and $4k$ sites allow a shift within the tetragonal basal plane. Relaxing the $1d$ position of Br ions into the direction along the tetragonal axis (c axis) into the Wykoff position, $2h$ does not lead to any improvement of the refinement or reduction of the ADP. This confirms that the Br displacement occurs only within the ab-plane (Cu-Br layer). The splitting of the O1 position $2f$ (0, $1/2$, 0) appears as well within the tetragonal basal plane with a statistical occupation of the Wykoff site $4n$ (x, $1/2$, 0). The final refinement, including the split Br ($4o$ or $4k$ sites) and O1 ($4n$) positions, leads to normal ADPs and is shown in Fig. 1. The crystallographic parameters (atomic positions, isotropic thermal parameters) as well as the most important interatomic distances, determined from the high-resolution data at RT, are given in Table I.

We have to recall here that for $(CuBr)Sr_2Nb_3O_{10}$ the tetragonal symmetry is preserved and that the originally proposed space group $P4/mmm$ with a square planar lattice of Cu atoms is still a valid description of the structure. In general, the deviations from the tetragonal symmetry can be detected in diffraction data not only through a splitting of certain Bragg peaks but also through the appearance of superlattice peaks. In the case of the $n = 2$ compound $(CuCl)LaNb_2O_7$, an orthorhombic splitting was observed in high-resolution synchrotron XRD while no splitting was detectable for $(CuCl)LaTa_2O_7$ by XRD.[5,11] Neutron-diffraction data for both compounds revealed, however, weak superlattice reflections, which are indexable in a four times larger unit cell with

TABLE I. Crystallographic data for $(CuBr)Sr_2Nb_3O_{10}$.

Atom	Site	x	y	z	100 U_{iso} (Å^2)
Cu	1*b*	0	0	0	1.4(1)
Br[a]	4*o*	1/2	0.422(3)	1/2	1.8(3)
Br[a]	4*k*	0.445(2)	0.445(2)	1/2	1.8(3)
Sr	2*h*	1/2	1/2	0.1404(2)	0.3(1)
Nb	1*a*	0	0	0	0.8(1)
Nb	2*g*	0	0	0.2732(1)	0.2(1)
O1[b]	4*n*	0.111(1)	1/2	0	0.4(1)
O2	2*g*	0	0	0.1196(2)	0.7(1)
O3	4*i*	0	1/2	0.2469(2)	0.5(1)
O4	2*g*	0	0	0.3833(2)	0.9(1)
Distance (Å)	Br on 4*o*	Br on 4*k*			
Cu-Br	2.975(9)	3.054(7)			
	2.547(8)	2.769(7)			
		2.452(7)			
Cu-O2	1.863(3)	1.863(3)			

[a]Site occupancy of Br at either 4*o* or 4*k* is 0.25.
[b]Site occupancy of O1 at 4*n* is 0.5.

$2a_t \times 2b_t \times c$.[1,5] For $(CuBr)Sr_2Nb_3O_{10}$, the high intensity data of D20 were, therefore, used to verify and to confirm the absence of any superlattice reflections at RT and low temperatures (2 K). As a conclusion, one can state that the average crystal structure of $(CuBr)Sr_2Nb_3O_{10}$ stays tetragonal in space group $P4/mmm$ over the studied temperature range between RT and 2 K. However, there exists a strong disorder of the Br atoms (within the Cu-Br layers) and of one of the oxygen atoms (within the NbO_6 perovskite blocks), which lowers the symmetry locally. Figure 2 displays this structure that leads to strong local deviations from a simple quadratic coordination of Br by Cu ions as the Br atom is statistically shifted from the center of the surrounding Cu square. The refinement does not allow deciding between an occupation of the 4*o* (x, 1/2, 1/2) or the 4*k* (x, x, 1/2) sites. With respect to the strong tendency of the d^9 ($t_{2g}^6 e_g^3$) Cu^{2+} ion to induce a Jahn-Teller distortion of the coordinating octahedra, the occupation of the 4*o* site seems to be more likely, as it leads to the formation of CuO_2Br_4 octahedra possessing two short and two long Cu-Br basal bonds [Fig. 2(b)]. However, the next-nearest neighbor interactions J_2 along the two diagonal directions remain equal [Fig. 2(b)], and the simple J_1-J_2 model could stay valid in this case. Figure 2(c) shows that a shift into the 4*k* position results in three different Cu-Br distances. In this case, the next-nearest neighbor interactions J_2 are different due to two geometrically different superexchange pathways J_2 and J_2' along the two diagonals within each square invalidating thereby the picture of the simple J_1-J_2 square lattice model for $(CuBr)Sr_2Nb_3O_{10}$.

B. Magnetic structures

The magnetic structures of $(CuBr)Sr_2Nb_3O_{10}$ were studied as function of magnetic field and temperature using the high-intensity data taken on D20. Due to the very low intensity of the magnetic scattering as compared to that of the nuclear scattering, the magnetic peaks are only visible in the difference patterns. The magnetic difference patterns are obtained by subtraction from the relevant patterns of a pattern recorded at 15 K under zero magnetic field (within the paramagnetic phase). Using the crystallographic model and the atomic coordinates, as determined from the high-resolution D2B data at 20 K, this zero field 15 K nuclear-background pattern was refined. The so-determined scale factor served in the following for the refinement of the difference spectra. Figure 3(a) displays parts of the difference pattern at 2 K recorded for magnetic fields of $H = 0$, 1, and 2.5 T. Magnetic peaks visible at 1 T are similar to those at zero field and correspond to the AF1 phase, with a magnetic propagation vector $\kappa_1 = [0\ 3/8\ 1/2]$, already described in our previous paper.[6] The refinement using the same magnetic structure model as used in Ref. 6 for the zero-field data works nicely and results in a magnetic moment value of $\mu_{Cu} = 0.75(2)\ \mu_B$. In this AF1 structure, spins are propagating in a cycloidal spiral within the Cu-Br layers with an AFM coupling between neighboring layers in c direction; for a picture of this magnetic structure, see Fig. 5 of Yusuf *et al.*[6] At 2.5 T, in addition to the existing peaks of the AF1 structure, new magnetic peaks at different scattering angles appear, which belong to a second AFM structure, AF2. The magnetic propagation vector of this AF2 phase is determined to $\kappa_2 = [0\ 1/3\ 0.49(3)]$[20] and corresponds, therefore, closely to the propagation vector [0 1/3 0.45(1)] found for data measured under a magnetic field of 4.5 T as mentioned in Ref. 6.

It is important to notice that the data taken under 2.5 T show the coexistence of AF1 and AF2 phases. Figure 3(b) shows the evolution of the magnetic peaks when applying higher magnetic field values. Under 5.5 T, the intensities of the peaks corresponding to the AF2-type structure ($\kappa_2 = [0\ 1/3\ 0.46(1)]$) have increased as compared to 2.5 T, while the peaks

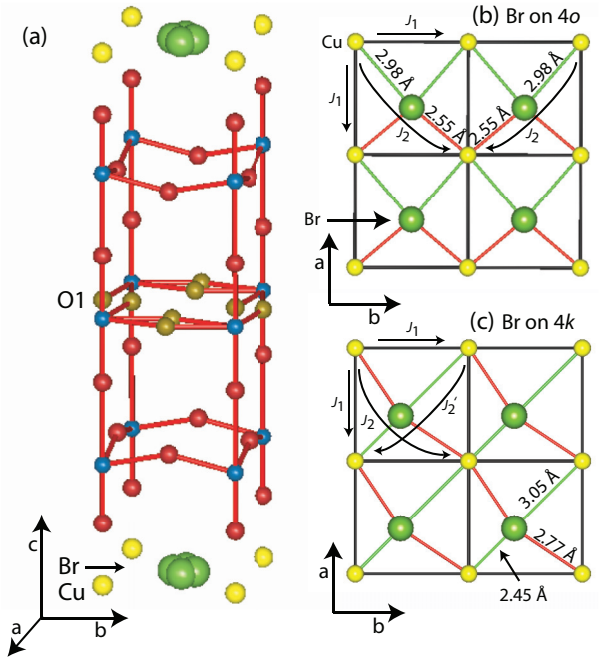

FIG. 2. (Color online) (a) Crystal structure of $(CuBr)Sr_2Nb_3O_{10}$. The Cu, Br, and Nb atoms are shown in yellow, green, and blue, respectively. The O atoms are shown in red except O1-atoms, which are shown in brown. The split Br 4*o* site and the split O1 4*n* site are also shown. Magnetic interaction pathways in the *ab* plane (Cu-Br-layer) with Br on one of the four statistically occupied sites, (b) 4*o* or (c) 4*k*, are also shown.

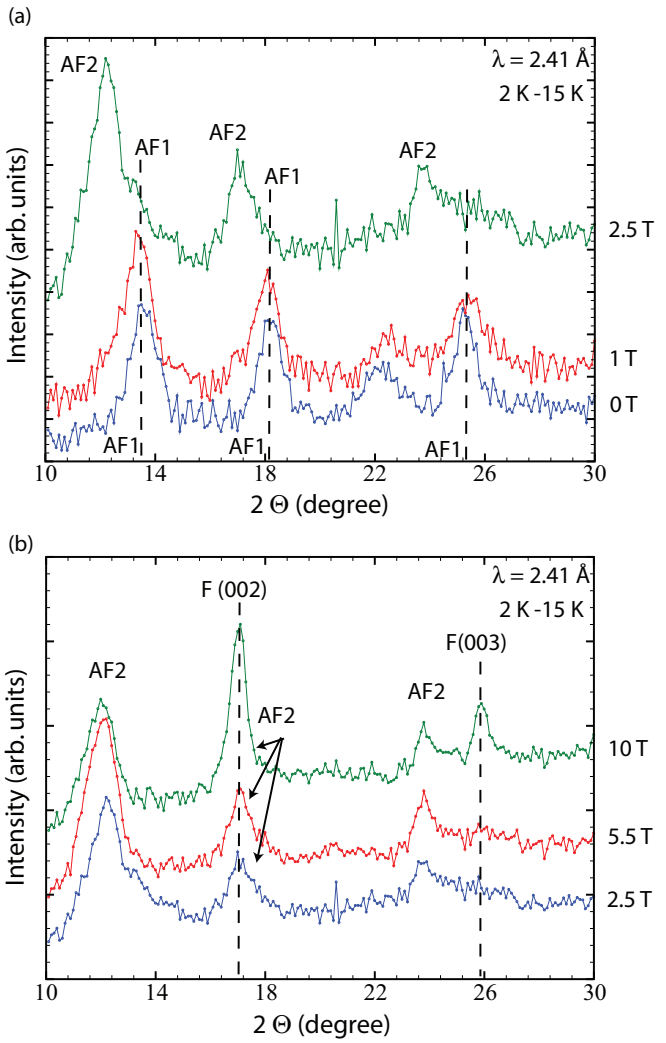

FIG. 3. (Color online) Magnetic diffraction patterns (after subtraction of the 15 K, 0 T diffraction pattern as nuclear background) as a function of magnetic field at 2 K showing the evolution of the different magnetic phases. For abbreviations see main text.

corresponding to the AF1 structure are no longer visible. Under the maximum applied field of 10 T, a further qualitative change becomes apparent with the strong appearance of ferromagnetic Bragg peaks ($\kappa_3 = [0\ 0\ 0]$) and a decrease of the intensity of the AF2-type peaks. The detailed analysis of the data reveals that the ferromagnetic phase (F) is, in fact, already present in the data taken at 5.5 and 4.5 T, a possibility already mentioned before for the 4.5 T data.[6]

Below we discuss the magnetic structure of the field-induced AF2 phase. Magnetic symmetry analysis was done using the program BASIREPS[18,19] for $\kappa_2 = [0\ 1/3\ \gamma]$ in space group $P4/mmm$. There are only two allowed irreducible representations (IRs), with IR1 having the basis vector [1 0 0] and IR2 having the basis vectors [0 1 0] and [0 0 1]. It was not possible to refine the magnetic-peak intensities of the AF2-type magnetic structure by assuming a sine-wave amplitude modulated structure having only one component (basis vector) for the spin direction. A good fit was achieved using a helix having two equal components in the [1 0 0] and the [0 0 1] directions. The corresponding magnetic

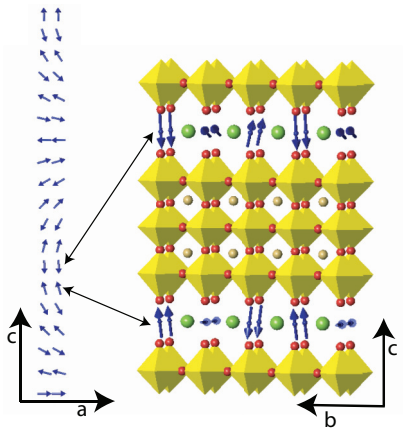

FIG. 4. (Color online) AF2 structure with $\kappa = [0\ 1/3\ 0.45]$; magnetic moments are confined in the ac plane forming a cycloidal spiral. Along the b axis, the spins turn by 120° between neighboring unit cells.

structure can be visualized as a cycloidal modulation of constant moment spins rotating within the ac-plane and is shown in Fig. 4. Using powder data, it is in principle not possible to discriminate between a helix and a sine-wave structure having the same components. If, however, the maximum amplitude of the magnetic moment in the sine-wave model is physically not reasonable, it is possible to exclude this model. This seems to be the case for $(CuBr)Sr_2Nb_3O_{10}$ where the refinement of the 5.5 T data using the helix model results in $\mu_{Cu} = 0.77(2)\ \mu_B$, whereas the sine-wave model using the same two basis vectors [1 0 0] and [0 0 1] gives $\mu_{Cu} = 1.09(3)\ \mu_B$. The moment value $\mu_{Cu} = 1.09(3)\ \mu_B$ is too large for Cu^{2+} especially in the titled low-dimensional and partly frustrated system.

The clear presence of the $(00l)$ reflections in the data taken at 10 T and the observed magnetic moment value of 0.8 μ_B, which is in accordance with the maximum moment in the AF1 and AF2 magnetic structures, indicates that the magnetic moments of the ferromagnetic phase are aligned within the Cu-halide layers. This does not rule out the possibility of a small c component for the magnetic moment not detectable in the current experiment.

With the knowledge of the three different magnetic structures, AF1, AF2, and F, the quantitative analysis of the purely magnetic diffraction patterns under different magnetic fields at 2 K has been performed to determine the degree of coexistence of these three magnetic phases. Figure 5 displays the results of the Rietveld refinements of the purely magnetic (difference) patterns under different magnetic fields at 2 K. Table II lists the determined magnetic-moment values for each phase as a function of magnetic field. One has to recall here that the magnetic moment values are determined using the scale factor determined from the refinement of the nuclear phase. In the case of coexisting magnetic phases, it is normally not possible to say whether the magnetic phases are present in different parts of the sample volume or whether they each embrace the whole sample volume. Only the presence of a strong magnetostriction effect, which would lead to nuclear phases having crystallographic unit cell parameters different for the different magnetic phases, would allow the determination of different scale factors and thereby the determination of

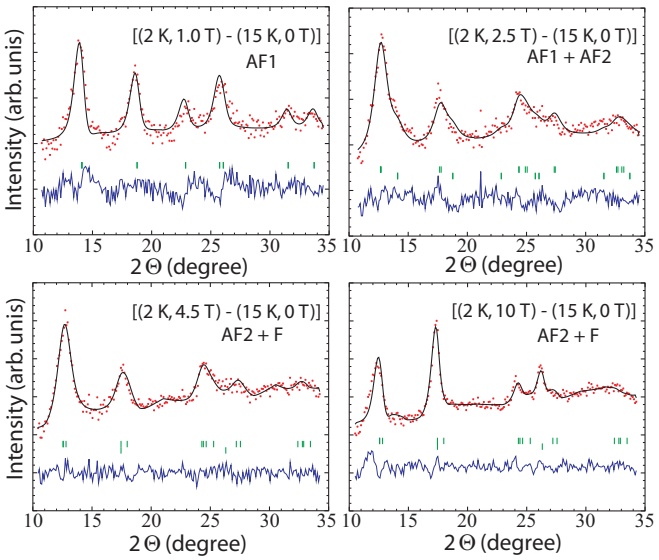

FIG. 5. (Color online) Rietveld refined magnetic diffraction patterns after subtraction of 15 K, 0 T diffraction pattern as nuclear background at 2 K under 1, 2.5, 4.5, and 10 T magnetic field. Observed, calculated, and difference patterns are shown by red points, black lines, and blue line, respectively. The calculated positions of the Bragg peaks are shown by vertical bars.

the relative phase fractions. As this is not the case in $(CuBr)Sr_2Nb_3O_{10}$, one has to take the determined magnetic moment values as the measure for the phase fraction. This seems all the more justified as the three different magnetic structures see the same maximum magnetic moment of about $\mu_{Cu} = 0.8\,\mu_B$ for the Cu^{2+} spin in those regions of the magnetic phase diagram where they are unique or strongly dominant, namely at 0 T for the AF1 phase, 4.5 T for the AF2 phase, and 10 T for the F phase. Keeping this in mind, Fig. 6 represents a magnetic phase diagram deduced using the values listed in Table II.[21]

Now we discuss the phase diagram in details. Several observations can be made looking at the magnetic field dependence of the magnetic structures displayed in Fig. 6. With increasing magnetic field, the zero-field AF1 phase first persists (1 T), then decreases (2.5 T), and has disappeared at 4.5 T. The field-induced AF2 phase does not yet appear at 1 T, although it already represents the majority phase at 2.5 T. With further increasing field, the AF2 phase decreases significantly between 5.5 and 10 T, corresponding to the magnetic field range where the F phase increases strongly. The F phase starts to be noticeable in the data taken at 4.5 T but could be already

TABLE II. Magnetic moment values of the different magnetic phases at 2 K as determined from the refinement of the difference spectra (after subtraction of the 15 K, 0 T pattern as nuclear background).

H (T)	0[a]	1	2.5	4.5	5.5	10
AF1 (μ_B)	0.79(1)	0.75(2)	0.43(3)	–	–	–
AF2 (μ_B)	–	–	0.71(2)	0.78(4)	0.77(2)	0.53(2)
F (μ_B)	–	–	–	0.27(7)	0.31(4)	0.80(2)
R_{Mag} (%)	3.7	7.4	13.5//2.8	2.1//3.4	5.6//7.0	13.5//2.1

[a]From Ref. 6.

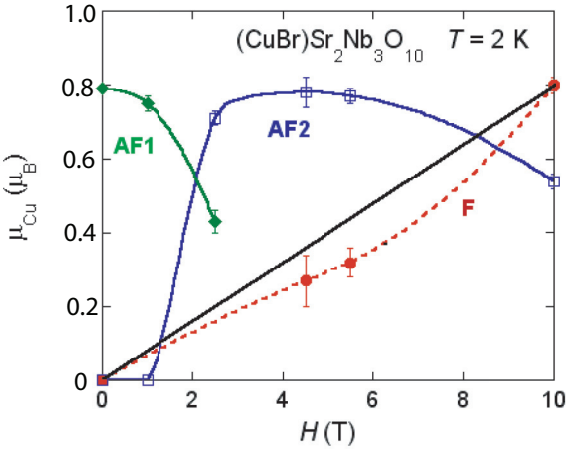

FIG. 6. (Color online) Magnetic moment values at $T = 2$ K, determined from the refinement of the difference spectra. The AF1 phase corresponds to the antiferromagnetic structure with $\kappa = [0\ 3/8\ 1/2]$, the AF2 phase corresponds to the one with $\kappa = [0\ 1/3\ \gamma]$, and the F phase corresponds to the ferromagnetic structure.

present at lower fields at a level not detectable by the present neutron data.

Based on these observations, it is now possible to deduce the scenario responsible for the appearance of the 1/3 magnetization plateau found in Ref. 13 for $(CuBr)Sr_2Nb_3O_{10}$. The AF1 phase is partly replaced under the effect of low magnetic fields by the simple F, which is characterized by the magnetic propagation vector $\kappa_3 = [0\ 0\ 0]$. This phase does not correspond to the phases proposed in Ref. 13 for the 1/3 magnetization plateau, having either $\kappa = [1/3\ 0\ 0]$ or $[1/6\ 1/3\ 0]$. In this low field region, the coexistence of AF1 and field-induced F phases leads to an increase of the magnetization with increasing field. However, due to the low phase fraction of the ferromagnetic phase, the peaks corresponding to the F phase are not yet visible in the neutron data. With increasing magnetic field, one enters above ~1.5 T the region of the magnetic phase diagram depicted in Fig. 4 of Ref. 13, which is called the 1/3 plateau phase, where the increase of the magnetization with increasing magnetic field slows down considerably. The neutron data show that this region is mainly determined by the coexistence of F and AF2 phases. The AF2 phase appears rapidly for magnetic fields higher than 1–2 T, replaces completely the AF1 phase, and at the same time slows down the formation of F. This slowing down of the formation of the F phase is best seen when comparing the determined value for the magnetic moment of the F phase at 5.5 T of $\mu_{Cu} = 0.31(4)\mu_B$ (Table II) to the value of 0.44 μ_B, expected for a linear increase (Fig. 6) of the moment between 0 and 10 T. The difference between the values of 0.31 μ_B and 0.44 μ_B seems at first sight not very large. However, since the scattering is proportional to the square of the magnetic moment, this difference in the moment values leads to a twofold increase of the magnetic intensity stemming from the F phase and therefore to a significant decrease in the goodness of fit of the neutron-diffraction pattern. Increasing the magnetic field to values higher than 5.5 T, the AF2 phase starts to decrease and gives way to an accelerated formation of F. This means that the appearance of the plateau in the magnetization curves shown

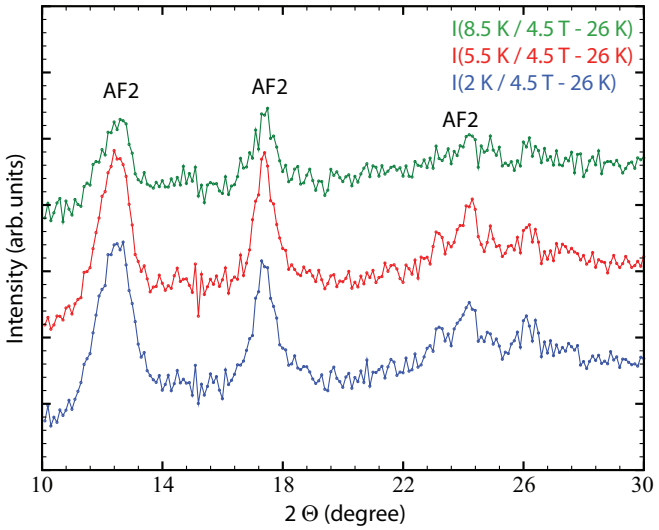

FIG. 7. (Color online) Magnetic peaks of the AF2-type magnetic structure at a magnetic field of 4.5 T showing the persistence of this magnetic phase up to $T > 8$ K.

in Ref. 13 is only coincidentally centered at a magnetization of 1/3 of the saturation magnetization. It cannot be related to the possible 1/3 plateau predicted within the J_1-J_2-J_3 model.[16] Its position depends solely on the magnetic field-dependent energy balance between the AF2 and F phases. In this context, it seems interesting to note that in the similar compound $(CuBr)Ba_2Ta_3O_{10}$, the plateau in the magnetization curve, displayed in Ref. 8, seems to be centered more at about $M = 0.27\ M_S$ not at 1/3 M_S.[22] This supports our view of the coincidental character of the magnetization plateau at 1/3 M_S in the title compound.

One has to point out that the intermediate magnetic field-induced AF2 phase governing the magnetization plateau is furthermore not related to the zero-field magnetic AF1 phase in a simple way, as not only the values but also the directions of the components of the magnetic propagation vectors are different. The possibility to identify the AF2 phase as the magnetic phase responsible for the formation of the 1/3 plateau phase is supported by its temperature dependence as well. Figure 7 displays that the magnetic Bragg peaks (characteristic for the AF2 phase) at 4.5 T are still present at 8.5 K. This mirrors the temperature dependence of the 1/3 plateau phase shown in Fig. 4 of Ref. 13, which shows a maximum at this magnetic field value in opposition to the zero-field AF1 phase, which disappears already for $T > 7.5$ K.

IV. CONCLUSIONS

High-resolution and high-intensity neutron-diffraction data indicate that, contrary to some $n = 2$ members of the Dion-Jacobson series $(CuX)A_{n-1}B_nO_{3n+1}$, the average crystal structure of the $n = 3$ compound $(CuBr)Sr_2Br_3O_{10}$ does not show any signs of deviation from the tetragonal symmetry described in space group $P4/mmm$. The existence of a statistical distribution of the halide over a split site, however, disturbs the symmetrical surrounding of the Cu^{2+} ions by Br ions in the Cu-Br layers and calls for a magnetic interaction model going beyond the simple J_1-J_2 model.

The present detailed temperature and magnetic field-dependent neutron-diffraction investigation allows us to conclude that the existence of a plateau in the magnetization curve of $(CuBr)Sr_2Nb_3O_{10}$ is only coincidentally situated at $M = 1/3\ M_S$. Under the effect of the magnetic field, the zero-field AF1 phase is replaced by a simple ferromagnetic phase, the formation of which is, however, slowed down by the appearance of an AF2 phase, which is stable at intermediate field values. AF1 and AF2 phases have strongly differing magnetic propagation vectors and therefore, are not directly related.

ACKNOWLEDGMENTS

A part of this work was supported by FIRST program from JSPS. Support from EPSRC, STFC, and the Royal Society is also acknowledged.

*Corresponding author: smyusuf@barc.gov.in
†Present address: Helmholtz Zentrum Berlin für Materialien und Energie, D-14109 Berlin, Germany.

[1] C. Tassel, J. Kang, C. Lee, O. Hernandez, Y. Qiu, W. Paulus, E. Collet, B. Lake, T. Guidi, M.-H. Whangbo, C. Ritter, H. Kageyama, and S.-H. Lee, Phys. Rev. Lett. **105**, 167205 (2010).
[2] A. A. Tsirlin and H. Rosner, Phys. Rev. B **82**, 060409(R) (2010).
[3] O. J. Hernandez, C. Tassel, K. Nakano, W. Paulus, C. Ritter, E. Collet, A. Kitada, K. Yoshimura, and H. Kageyama, Dalton Trans. **40**, 4605 (2011).
[4] A. A. Tsirlin, A. M. Abakumov, C. Ritter, P. F. Henry, O. Janson, and H. Rosner, Phys. Rev. B **85**, 214427 (2012).
[5] A. A. Tsirlin, A. M. Abakumov, C. Ritter, and H. Rosner, Phys. Rev. B **86**, 064440 (2012).
[6] S. M. Yusuf, A. K. Bera, C. Ritter, Y. Tsujimoto, Y. Ajiro, H. Kageyama, and J. P. Attfield, Phys. Rev. B **84**, 064407 (2011).
[7] T. A. Kodenkandath, J. N. Lalena, W. L. Zhou, E. E. Carpenter, C. Sangregorio, A. U. Falster, W. B. Simmons, Jr., C. J. O'Connor, and J. B. Wiley, J. Am. Chem. Soc. **121**, 10743 (1999).
[8] Y. Tsujimoto, H. Kageyama, Y. Baba, A. Kitada, T. Yamamoto, Y. Narumi, K. Kindo, M. Nishi, J. P. Carlo, A. A. Aczel, T. J. Williams, T. Goko, G. M. Luke, Y. J. Uemura, Y. Ueda, Y. Ajiro, and K. Yoshimura, Phys. Rev. B **78**, 214410 (2008).
[9] H. Kageyama, T. Kitano, N. Oba, M. Nishi, S. Nagai, K. Hirota, L. Viciu, J. B. Wiley, J. Yasuda, Y. Baba, Y. Ajiro, and K. Yoshimura, J. Phys. Soc. Jpn. **74**, 1702 (2005).
[10] N. Oba, H. Kageyama, T. Kitano, J. Yasuda, Y. Baba, M. Nishi, K. Hirota, Y. narumi, M. Hagiwara, K. Kindo, T. Sato, Y. Ajiro, and K. Yoshimura, J. Phys. Soc. Jpn. **75**, 113601 (2006).
[11] A. A. Tsirlin, A. M. Abakumov, G. Van Tendeloo, and H. Rosner, Phys. Rev. B **82**, 054107 (2010).
[12] S. Furukawa, T. Dodds, and Y. B. Kim, Phys. Rev. B **84**, 054432 (2011).
[13] Y. Tsujimoto, Y. Baba, N. Oba, H. Kageyama, T. Fukui, Y. Narumi, K. Kindo, T. Saito, M. Takano, Y. Ajiro, and K. Yoshimura, J. Phys. Soc. Jpn. **76**, 063711 (2007).
[14] A. Honecker, J. Schulenburg, and J. Richter, J. Phys.: Condens. Matter **16**, S749 (2004).

[15] A. Honecker, Can. J. Phys. **79**, 1557 (2001).
[16] L. Seabra, N. Shannon, P. Sindzingre, T. Momoi, B. Schmidt, and P. Thalmeier, J. Phys.: Conference Series **145**, 012075 (2009).
[17] J. Rodriguez-Carvajal, Physica B **192**, 55 (1993).
[18] Full Prof Suite, http://www.ill.eu/sites/fullprof/.
[19] C. Ritter, Solid State Phenom. **170**, 263 (2011).
[20] Due to the tetragonal symmetry, it is not possible to discriminate from powder-diffraction data between the magnetic propagation vectors $\kappa_2 = [0\ 1/3\ \gamma]$ and $\kappa_2 = [1/3\ 0\ \gamma]$.
[21] Instead of assuming a coexistence of AF2 and F magnetic phases in spatially different regions, it is also possible to explain the neutron data if the AF2 phase has an additional ferromagnetic component. This does not change the following discussion concerning the 1/3 magnetization plateau; however, in Fig. 6, one would have to regard AF2 and F phases, respectively, as AFM and ferromagnetic components of the same phase. However, the magnetization data indicate that the F phase is induced as soon as a field is applied, whereas the AF2 phase seems to appear only above $\sim$1 T, which favors the two-phase model.
[22] Unpublished data of Tsirlin *et al*. show that (CuBr)$Ba_2Ta_3O_{10}$ adopts under a magnetic field the same AF2-type magnetic structure as (CuBr)$Sr_2Nb_3O_{10}$.